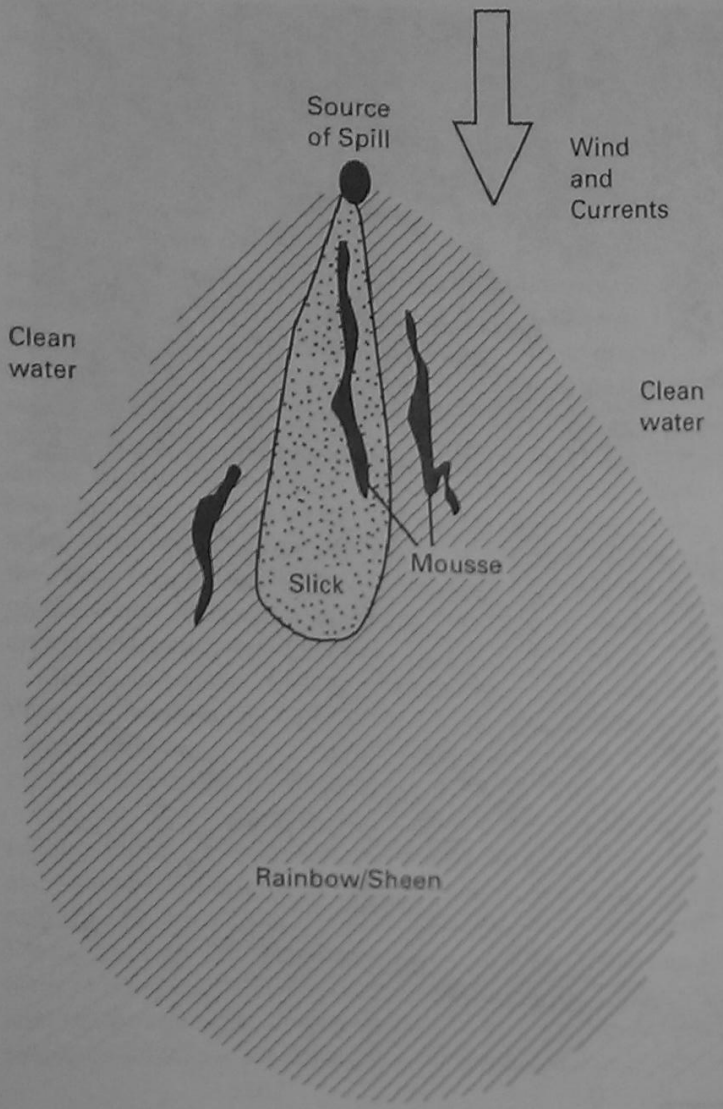

Figure 9-29 Diagram showing the characteristics of a typical oil spill.

Rainbow Very thin iridescent multicolored bands visible on the water surface.

Rainbow/sheen Two categories commonly lumped together because they are volumetrically insignificant and are difficult to distinguish.

Figure 9-29 shows the distribution and relative extent of these components in a typical oil spill, where 90 percent of the volume is concentrated in 10 percent of the area, largely in the form of slicks and mousse. Table 9-4 lists the interactions between oil and electromagnetic energy at wavelength regions ranging from UV through radar. Figure 9-30 shows these interactions diagramatically for oil and water to explain their different signatures. The following sections describe the detection of oil slicks on images acquired in the various spectral regions.

UV Images Figure 9-30A shows that incoming UV radiation from the sun stimulates fluorescence in oil. Figure 9-31 shows spectral radiance curves for water (solid) and a thin layer of oil (dashed). The higher radiance of oil at wavelengths of 0.30 to 0.45 μm (long-wavelength UV to visible blue) is due to fluorescence. Individual crude oils and refined products have peak fluorescence at different wavelengths that depend upon composition and weathering of the hydrocarbons. Figure 9-32 is a daytime image acquired by a cross-track aircraft scanner equipped with a UV detector (using wavelengths of 0.32 to 0.38 μm). The area is the Santa Barbara Channel off the coast of southern California, where numerous natural oil seeps occur on the seafloor and form widespread slicks on the surface. Fluorescence from the oil slicks at UV wavelengths causes the bright signatures in the image. The platforms shown in the image are oil production facilities.

UV images are the most sensitive remote sensing method for monitoring oil on water and can detect films as thin as 0.15 μm (Maurer and Edgerton, 1976). Daylight and very clear atmosphere are necessary to acquire UV images. UV energy is

Table 9-4 Remote sensing of oil spills

Spectral region	*Oil signature*	*Oil property detected*	*Imaging requirements*	*False signatures*
UV, passive (0.3 to 0.4 μm)	Bright	Fluorescence stimulated by sun	Day; good weather	Foam
UV, active (0.3 to 0.4 μm)	Bright	Fluorescence stimulated by laser	Day and night; good weather	Foam
Visible and reflected IR (0.4 to 3.0 μm)	Bright—mousse Dark—slick Bright—sheen	Reflection and absorption of sunlight	Day; good weather	Wind slicks, discolored water
Thermal IR (8 to 14 μm)	Bright—mousse Dark—slick	Radiant temperature controlled by emissivity	Day and night; good weather	Warm and cool currents
Radar (3 to 30 cm)	Dark	Dampening of capillary waves	Day and night; all weather	Wind slicks, current patterns

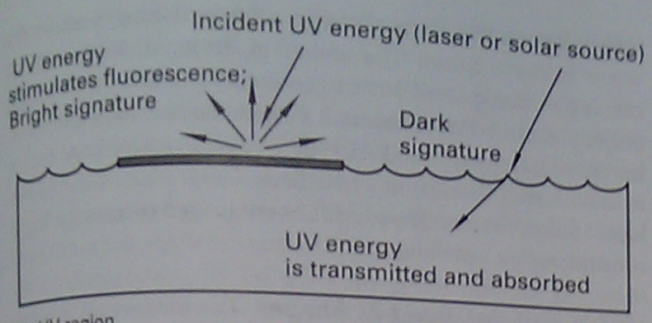

A. UV region.

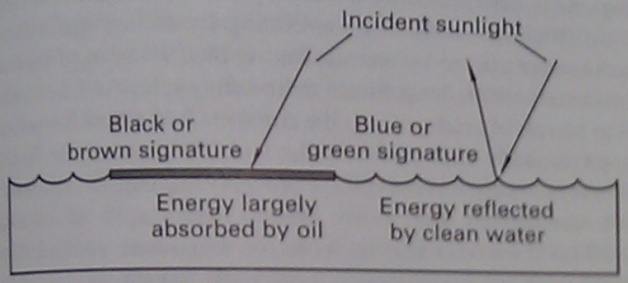

B. Visible and reflected IR regions.

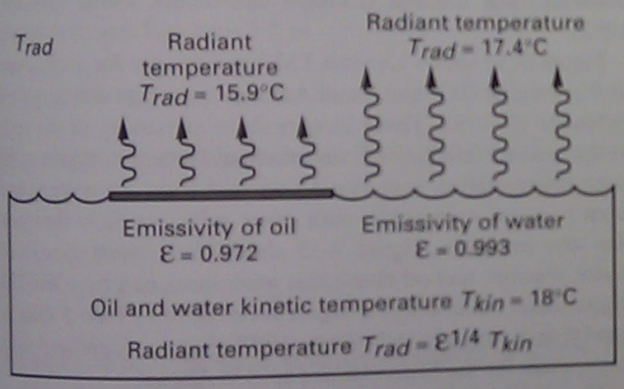

C. Thermal IR region.

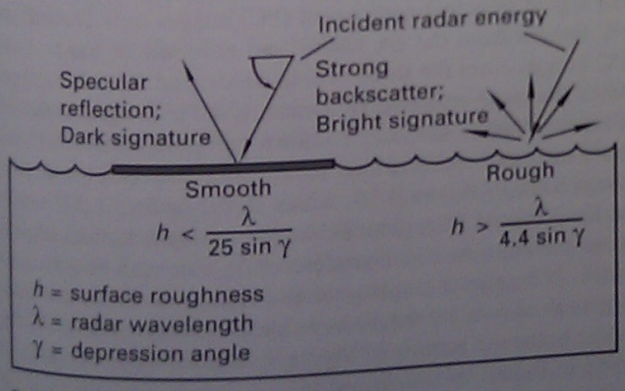

D. Radar region.

Figure 9-30 Interaction mechanisms among oil, water, and electromagnetic energy at different wavelength regions.

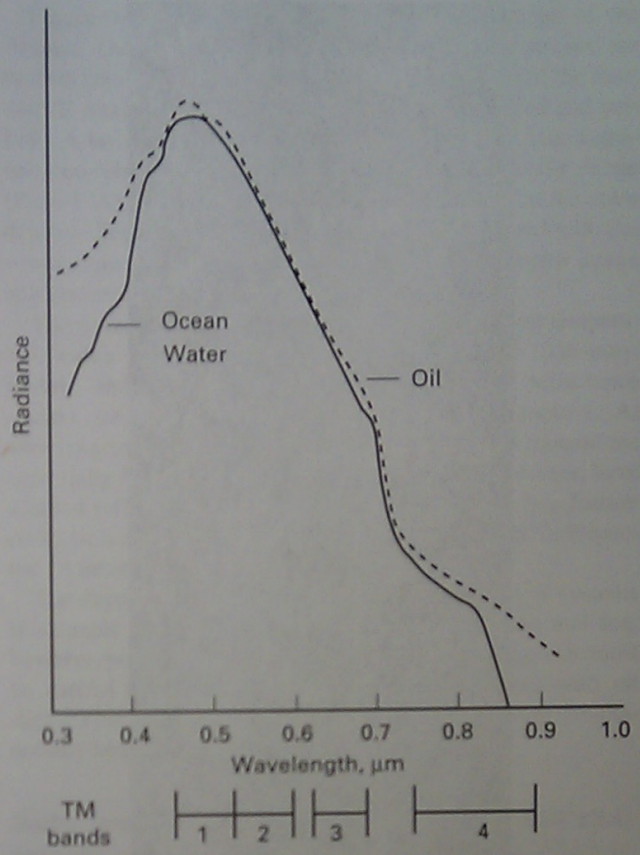

Figure 9-31 Spectral radiance for ocean water and a thin film of oil. From Vizy (1974, Figure 5).

strongly scattered by the atmosphere but usable images can be acquired at altitudes below 1000 m. Floating patches of foam and seaweed have bright UV signatures that may be confused with oil (Table 9-4). Foam and seaweed can be recognized on images in the visible band acquired simultaneously with the UV images.

Figure 9-32 is a passive image that records energy stimulated by the sun. Active UV systems have been developed for aircraft use. A laser irradiates the water with UV energy that stimulates any oil to fluoresce. The fluorescence is recorded as a spectrum, rather than an image. The spectrum can be compared with a reference library of spectra to identify the unknown hydrocarbon. These active systems can acquire images both day and night. O'Neil, Buja-Bijunas, and Rayner (1980) describe a system the Canadian government used to monitor oil pollution. Quinn and others (1994) describe an active system developed for the Kuwait government.

The British Petroleum Company used an active UV system, called *airborne laser fluorosensor* (ALF), for oil exploration in offshore basins around the world. Many oil accumulations leak

Figure 9-32 UV scanner image (0.32 to 0.38 μm) of natural oil seeps in the Santa Barbara Channel, California, July 31, 1974. Bright signatures are fluorescence stimulated by sunlight interacting with the oil. From Maurer and Edgerton (1976, Figure 9).

hydrocarbons that form slicks in offshore basins, such as the Santa Barbara Basin. The ability to detect slicks by remote sensing in unexplored basins can contribute to an exploration project. British Petroleum and Pertamina (the Indonesian national oil company) used ALF to survey seven offshore basins in Indonesia (Thompson and others, 1991). Six of the basins have slicks; three of those basins were judged to have the highest exploration potential.

Visible and Reflected IR Images The interaction between oil and electromagnetic energy in the visible and reflected IR regions is determined by the absorption and reflection of sunlight (Figure 9-30B). A complicating factor is sunglint from calm water caused by the oil. During their invasion of Kuwait in January 1991, Iraqi forces deliberately released 4 to 6 million barrels of crude oil into the Arabian Gulf, where it covered approximately 1200 km^2 of water and 500 km along the Saudi Arabian coastline. This spill is probably the largest in history; for comparison the 1989 *Exxon Valdez* spill in Alaska (<300,000 barrels) was an order of magnitude smaller. The Iraqis also set fire to onshore oil wells, which created giant smoke plumes and spilled additional oil onto the desert. The smoke plumes were tracked on images from AVHRR, Meteosat, and Landsat (Limaye and others, 1992; Cahalan, 1992).

Figure 9-33 shows Landsat TM-band images for a subscene of the Arabian Gulf and Saudi Arabian coast that was acquired February 16, 1991. These images show signatures of the spill in the visible, reflected IR, and thermal IR bands. Figure 9-34 is an interpretation map that I prepared from the images and from personal experience with other spills; no field information was available. Figure 9-35 shows reflectance spectra of water, mousse, and oil sheen that were measured from the TM digital data. Mousse has a higher reflectance in band 5 than in band 4 or 7. Stringer and others (1992, Figure 14) showed similar spectra for the *Exxon Valdez* spill in Alaska.

The individual TM bands of the Arabian Gulf spill were digitally processed to extract additional information. Three different sets of principal-component (PC) images were created: six PC images from the six visible and reflected IR bands, three PC images from the three visible bands, and three PC images from the three reflected IR bands. The PC images of the reflected IR bands 4, 5, and 7, shown in Figure 9-36A, B, C, extract the most information. This relationship is explained by the spectra in Figure 9-35, which have maximum differences in the reflected IR region. PC image 1 (Figure 9-36A) emphasizes the heaviest concentrations of mousse with bright signatures. PC image 2 emphasizes fine details of the mousse plus slick, as shown by the narrow black tendrils adjacent to the coast in the top portion of Figure 9-36B. Although PC image 3 (Figure 9-36C) is dominated by noise, the northwest-trending brighter patch is atmospheric haze or smoke. A number of band-ratio images were created, but in general these were not as effective as the PC images. In ratio 4/3 (Figure 9-36D) the

mousse is extracted with a bright signature that is comparable to PC image 1 (Figure 9-36A).

Plate 19A, B, C shows the combinations of individual TM bands that are most effective in discriminating the oil. In the 1-2-3 normal color image (Plate 19A) the dark signature of mousse is difficult to discriminate from the dark blue of water. Water penetration of these visible bands causes bright signatures from the shallow shoals (Figure 9-33H), which complicates interpretation. In the 4-5-7 image of reflected IR bands (Plate 19B), mousse has a distinctive bluish green signature. Mousse has a strong reflectance in band 5 (Figure 9-35), which is shown in green.

The National Geographic Society (Williams, Heckman, and Schneeberger, 1991) published an extensive collection of images and photographs of the environmental destruction caused in Kuwait by the Iraq invasion.

Thermal IR Images Figure 9-30C shows the interaction of thermal IR energy with oil and water. Both liquids have the same kinetic temperature because they are in direct contact. Chapter 5 points out that radiant temperature is a function of both radiant temperature and emissivity. Table 5-1 shows that the emissivity of water is 0.993, but a thin film of petroleum reduces water's emissivity to 0.972. Radiant temperature is calculated from Equation 5-8 as

$$T_{rad} = \varepsilon^{1/4} T_{kin}$$

For water at a kinetic temperature of 291°K (18°C), the radiant temperature is

$$T_{rad} = 0.993^{1/4} \times 291°K$$
$$= 290.5°K, \quad \text{or } 17.5°C$$

For an oil slick at the same kinetic temperature of 291°K, the radiant temperature is

$$T_{rad} = 0.972^{1/4} \times 291°K$$
$$= 288.9°K, \quad \text{or } 15.9°C$$

This difference of 1.6°C in radiant temperature between the oil (15.9°C) and water (17.5°C) is readily measured by thermal IR detectors, which are typically sensitive to temperature differences of 0.1°C. Figure 9-37 shows two images acquired by an aircraft multispectral scanner of an oil slick in the Gulf of Mexico off Galveston, Texas. The oil tanker *Burmah Agate* collided with another vessel, spilling crude oil. Figure 9-37B is a thermal IR image in which the oil slick has a cooler signature (darker) than the surrounding water (brighter signature). The warm streaks are caused by mousse, which reradiates absorbed sunlight at thermal IR wavelengths. The oil slick and mousse are identified much better in this thermal IR image than in the matching visible image (Figure 9-37A).

Figure 9-33F is a TM thermal IR band 6 image of the Arabian Gulf spill. The bright (warm) sinuous streaks are mousse. Plate 19D is a color density-sliced version of the thermal IR image. The mousse has warm signatures (red and yellow). A broad, northwest-trending cool band (dark blue signature) correlates with bright tones in the normal color image (Plate 19A) and is attributed to thin, high clouds. On the color density-sliced image, sinuous cool streaks associated with the warm mousse have dark signatures on the normal color image and are attributed to oil slicks.

The aircraft and TM images record a single radiant temperature value for oil over a broad spectral range. Salisbury, D'Aria, and Sabins (1993) measured thermal IR reflectance spectra for five oils, plus seawater, foam, and mousse. At wavelengths of 8 to 14 μm, spectra of the oils and mousse are essentially flat and featureless. Water and foam, however, have a broad reflectance minimum from 10 to 12 μm; this feature could be useful in discriminating oil from water on multispectral IR images such as TIMS.

The daytime and nighttime capability of thermal IR systems is valuable for surveillance around the clock. Rain and fog, however, prevent image acquisition. Also, the interpreter must be careful to avoid confusing cool water currents with oil slicks. This problem can be minimized by interpreting simultaneously acquired UV and IR images.

Radar Images Figure 9-30D shows that an oil slick eliminates the roughness caused by small-scale waves, which results in an area of low backscatter (dark signature) surrounded by the stronger backscatter (bright signature) from rough, clean water. Figure 9-38 shows the characteristic dark signatures of oil slicks on two ERS-1 images of European waters. ERS-1 radar images are particularly sensitive to differences in water roughness because of their steep depression angle and VV polarization. The Seasat image of the Santa Barbara coast shown in Chapter 7 accurately records the oil slicks. On SIR-A images, slicks are less apparent but can be enhanced by image processing (Estes, Crippen, and Star, 1985). Aircraft images are also effective for recognizing oil slicks.

Radar images may be acquired day or night under any weather conditions, which is an advantage over other remote sensing systems for monitoring oil spills. As with other images, however, radar images must be interpreted carefully, because dark streaks may be signatures of smooth water that is not caused by oil. Internal waves and shallow bathymetric features are two other possible causes of dark signatures. This problem can be reduced by comparing radar signatures with signatures on simultaneously acquired images in other wavelength regions.

Images of Other Oil Spills On June 3, 1979, the Ixtoc 1 offshore well in the Bay of Campeche, off the Yucatan Peninsula of Mexico, blew out and was not capped until March 24, 1980.